

# Variables in Globular Cluster NGC 5024

M. Safonova and C. S. Stalin

*Indian Institute of Astrophysics, Koramangala, Bangalore 560 034*

## ABSTRACT

We present the results of a commissioning campaign to observe Galactic globular clusters for the search of microlensing events. The central  $10' \times 10'$  region of the globular cluster NGC 5024 was monitored using the 2-m Himalayan Chandra Telescope in  $R$ -band for a period of about 8 hours on 24 March 2010. Light curves were obtained for nearly 10,000 stars, using a modified Difference Image Analysis (DIA) technique. We identified all known variables within our field of view and revised periods and status of some previously reported short-period variables. We report about eighty new variable sources and present their equatorial coordinates, periods, light curves and possible types. Out of these, 16 are SX Phe stars, 10 are W UMa-type stars, 14 are probable RR Lyrae stars and 2 are detached eclipsing binaries. Nine of the newly discovered SX Phe stars and two eclipsing binaries belong to the Blue Straggler Star (BSS) population.

*Subject headings:* globular clusters: general — globular clusters: individual (NGC 5024): variable stars

## 1. Introduction

Since the beginning of the modern-day astrophysics, globular clusters (GCs) have been a working laboratory for observers, providing invaluable information and serving as models for understanding stellar dynamics. With the recent discovery that most of the galaxies host massive/supermassive black holes in their centres, the question was raised of the dynamical detection of such black holes in low-mass, non-active stellar systems, of which GCs are potential candidates. The well-established correlations between the properties of the supermassive black holes and their host galaxies do suggest that, in extrapolation, globular clusters follow the same relations (Safonova & Shastri 2010). Most of the attempts in search of the central intermediate-mass black holes (IMBHs) in globular clusters, however, are not direct and present enormous observational difficulties due to the crowding of stars in the GC cores. Recently, Safonova & Stalin (2010) proposed a method of detection of the central IMBH in GCs by microlensing (ML) of the cluster stars. In 2010, we have initiated the observational programme to search for ML signatures using the 2.0-m Himalayan Chandra Telescope (HCT) at the In-

dian Astronomical Observatory (IAO), Hanle, and the 2.3-m Vainu Bappu Telescope (VBT) at the Vainu Bappu Observatory, Kavalur, both operated by the Indian Institute of Astrophysics (IIA), Bangalore. The programme consists of obtaining one set of observations each in  $V$  and  $I$  bands of a selected set of clusters every 15–20 days for the period of 5–7 years (Safonova & Stalin 2010). The globular cluster NGC 5024 (M53) was observed as part of the commissioning observations for this programme.

It is well known by now that any microlensing search yields a dataset suitable for detecting variable stars that are unrelated to ML events (for ex., Cook 2006). Moreover, it was also discovered that the regular ML observations are more efficient at finding faint variables, being insensitive to bright ones because of saturation. In this paper, we report the results of our commissioning observations. This data was used to establish our operational procedure and to tune and test the data reduction pipeline. The purpose was not to specifically discover the new variables with these observations but rather use the data to build the analytical tools for use with our full time-series database. The choice to observe the cluster M53 was made

based on convenience, as an accessible target at the time of observation, and on the possibility for scientific potential from studying the variable stars in the cluster. The details of the data set analyzed here are not identical to our main microlensing time-series dataset, but we can use these observations to test our ability to obtain high-quality photometry defined as light curves with low noise, both random and systematic, and to be able to discern astrophysical signals with the timescales and depth of typical GC stellar variability.

M53 ( $\alpha_{2000} = 13^{\text{h}}12^{\text{m}}55^{\text{s}}.3$ ,  $\delta_{2000} = +18^{\circ}10'9''$ ) is a moderately compact metal-poor with  $[\text{Fe}/\text{H}] = -2.04$  (Zinn 1985) outer halo globular cluster that is rich in RR Lyrae variables. Though M53 was studied extensively in the last decade being the second most abundant cluster in variable stars after M15, only variables of a pulsating type have been discovered. In the latest 2010 updated version of the catalogue of variables in M53 (Clement et al. 2001) there are 62 reported RR Lyrae (RR1) stars, 8 suspected long-period SR stars and 15 SX Phe stars. Out of almost 200 blue straggler stars (BSS) discovered so far in M53, Beccari et al. (2008) estimated some 14% to be in binary systems, however no eclipsing binaries were previously found in this cluster.

Despite the high variable content of M53 and a favourable position in the galaxy where both field contamination and interstellar reddening are very low,  $E(B - V) = 0.02$  (Schlegel et al. 1998), the only extensive time-series photometry study has been done recently by Dekany & Kovacs (2009) (hereafter referred to as DK). Previous studies were using the point spread function (PSF) fitting directly to the images, which does not allow precise measurements in crowded fields, limiting the possibility for detecting small-amplitude variables. In contrast, the Differential Image Analysis (DIA) is a powerful technique which allows accurate PSF photometry even in very crowded fields. In present work, we apply a new pipeline based on an improved version of the differential imaging analysis, developed by D. Bramich (2008), to a set of  $R$ -band images in order to search for variables down to  $R = 21$  mag. We have recovered all previously known variable stars in our field of view and revisited all known short-period SX Phe-type stars in an attempt to refine their periods and coordinates. We report new candidate variables,

determine the periods of new short-period variable stars, report candidate eclipsing binaries and flux variability amongst some of the Stetson’s photometrically standard stars. Some of the new variables were matched to the BSS stars discovered earlier by Beccari et al. (2008). The emphasis of this work is on the reporting the new short-period variable sources. The final characterization of the newly discovered variables, especially the detailed photometry of matched BSS based on their position on the color magnitude diagram (CMD) to estimate mass and temperature from isochrone fitting, will be presented in a future paper. This paper is composed as follows. Observations and data reduction are described in Section 2. In Section 3 we discuss previously known variables in M53, in Section 4 we describe the search for new variables, explain the methods we used to identify new variable stars (RR Lyrae, SX Phe, eclipsing binaries), list the properties of all newly detected variables and display their light curves, and in Section 5 we give the summary of our results.

## 2. Observations and Data Reduction

### 2.1. Observations

Photometric observations were obtained on March 24, 2010, using the Himalayan Faint Object Spectrograph and Camera (HFOSC) mounted on the 2.0-m HCT of the IAO, located at 4500 m above sea level. A total of 101 image frames, each of 100 secs exposure, were collected in  $R$ -band during continuous 8 hours of observations. HFOSC is equipped with a Thompson CCD of  $2048 \times 2048$  pixels with a pixel scale of  $0''.296/\text{pix}$  and a field of view of  $\sim 10' \times 10'$ . The readout noise, gain and readout time of the CCD are  $4.8 \text{ } \bar{e}$ ,  $1.22 \text{ } \bar{e}/\text{ADU}$ , and 90 sec, respectively.

A grey-scale map of a  $R$  CCD image (reference frame) is shown in Figure 1. It shows an area of about  $5.5' \times 5.5'$  of the total observed field. 16 confirmed SX Phe stars are represented by circles labelled with their respective designations given in Table 6. Figure 2 *Top* shows the positions of RR Lyrae, W UMa and eclipse candidates, and *Bottom* of unclassified type variables, respectively.

### 2.2. Data Reduction

To extract high precision photometry from the M53 image frames, we employed the DIA tech-

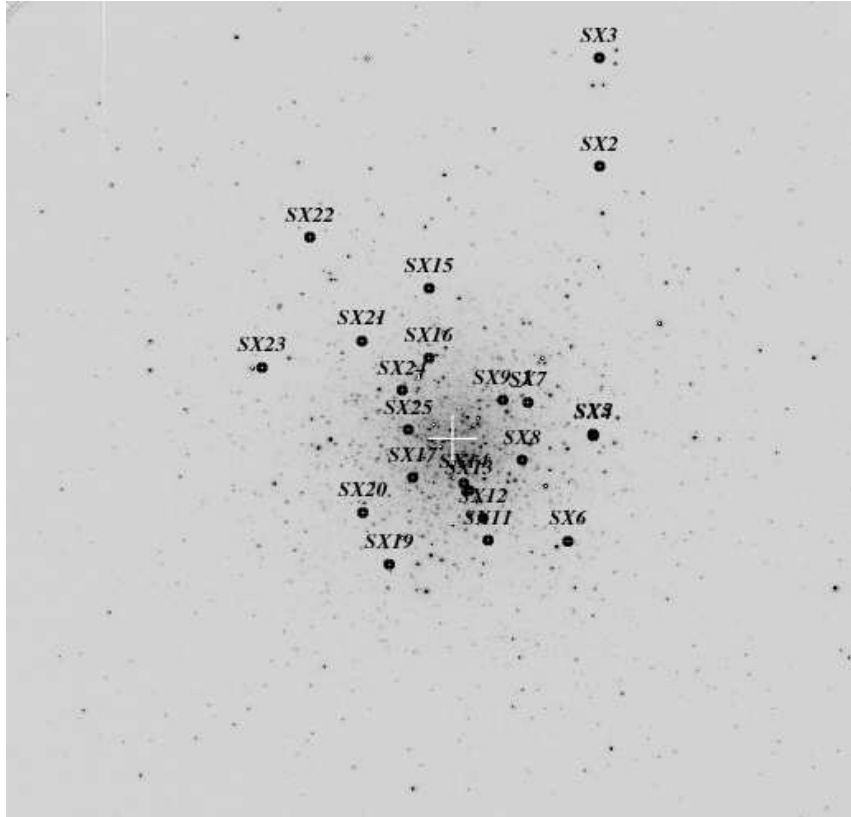


Fig. 1.—  $10 \times 10$  arcmin<sup>2</sup> grey-scale map of a  $R$  reference image of the globular cluster M53. 16 confirmed SX Phe stars are labelled by their respective designations given in Table 6. The image was scaled so that to only mark the positions of the stars. The cross marks the centre of the cluster. The cluster size is  $\sim 13'$ , thus we can be confident that most detected variables belong to the cluster. North is up, east to the left.

nique implemented through a pre-release version of the pipeline DanDIA. The idea of DIA is to obtain information about the brightness behaviour of a source by analyzing the difference between the image in each of the frames from the series and the image in a fixed reference image. This technique allows the extraction of high S/N signals even in the highly crowded central regions of globular clusters (Alard & Lupton 1998; Alard 2000; Bramich et al. 2005; Bramich 2008). We used a pre-release version of DanDIA<sup>1</sup> pipeline which includes a new algorithm that models the convolution kernel matching the PSF of a pair of images of the same field as a discrete pixel array (Bramich 2008). This procedure is well described in a series

of papers by Arellano Ferro et al. (2008).

Briefly, the raw image data is passed through a series of modules, starting with bias subtraction, flat-field corrections and cosmic rays removal. The gain and readout noise at the time of observations were calculated automatically at this stage. A reference frame (RF) was chosen out of the best-seeing pre-processed images, in which the FWHM of the PSF was measured to be  $\sim 3.77$  pixels. In the RF, the fluxes (referred to as reference fluxes) and positions of all PSF-like objects were measured by extracting a spatially variable (with polynomial degree 3) empirical PSF from the image and fitting this PSF to each detected object. The source detection threshold was set to  $3\sigma$  above the background. The detected stars in each image in the time-series were matched with those detected

<sup>1</sup>DanDIA is build from the DanIDL library of IDL routines (<http://www.danidl.co.uk>)

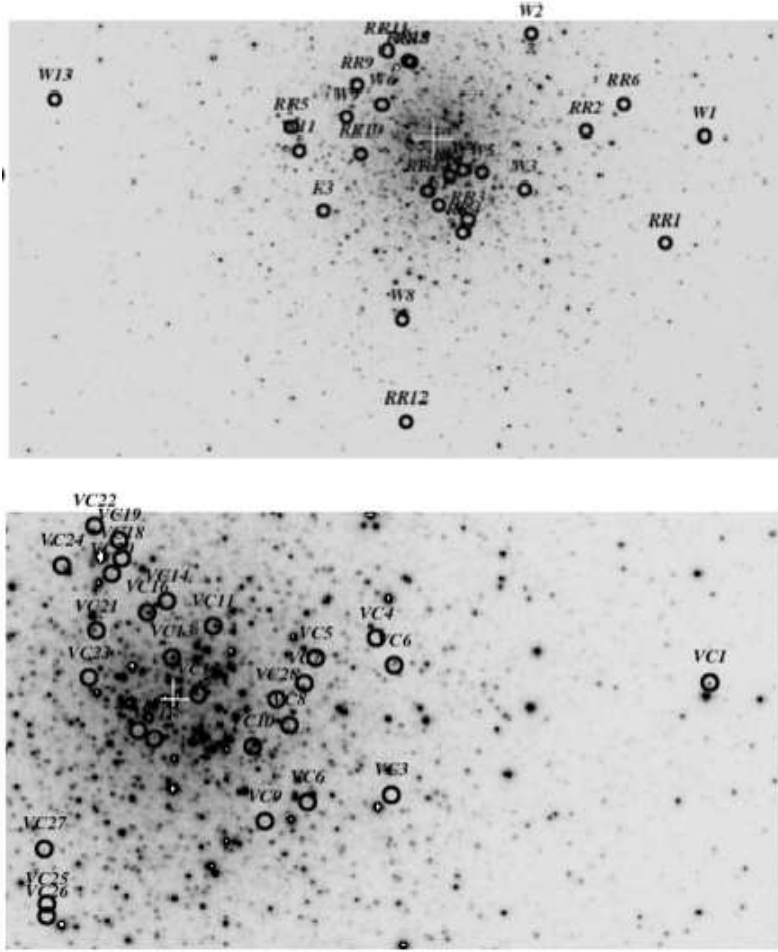


Fig. 2.— *Top*: Grey-scale map of a  $R$  reference image, covering an area of about  $4.0 \times 2.2$  arcmin<sup>2</sup>. Variable candidates are labelled by their respective designations given in Tables 7 and 8. *Bottom*: Grey-scale map of a  $R$  reference image, covering an area of about  $5 \times 3.5$  arcmin<sup>2</sup>. 28 uncertain-type variable candidates are labelled by their respective designations given in Table 9. The image was cropped and scaled so that to only mark the positions of the stars. The cluster size is  $\sim 13'$ , thus we can be confident that most variables belong to the cluster. The cross marks the centre of the cluster. North is up, east to the left.

in the RF, and a linear transformation was derived, which was used to register each image with the reference image.

Each registered image was split into  $6 \times 6$  grid of subregions and a set of kernels, modelled as pixel arrays, were derived matching each image subregion to the corresponding subregion in the RF. The kernel solution for each image pixel was determined by interpolating the grid of kernel models using bilinear interpolation. A series of difference images was created by subtracting the RF, con-

volved with an appropriate kernel solution, from each registered image.

Photometry on the difference images via optimal PSF scaling (Bramich et al. 2005) yielded light curves of differential fluxes for each star. The light curves were constructed by calculating the total flux  $f_{\text{tot}}(t)$  in ADU/s at each epoch  $t$  from

$$f_{\text{tot}}(t) = f_{\text{ref}} + \frac{f_{\text{diff}}(t)}{p(t)}, \quad (1)$$

where  $f_{\text{ref}}$  is the reference flux in ADU/s,  $f_{\text{diff}}(t)$

is the differential flux in ADU/s and  $p(t)$  is the photometric scale factor (integral of the kernel solution). Conversion to instrumental magnitudes was achieved using

$$m_{\text{instr}}(t) = 25.0 - 2.5 \log[f_{\text{tot}}(t)], \quad (2)$$

where  $m_{\text{instr}}(t)$  is the instrumental magnitude of the star at epoch  $t$ .

### 2.3. Post-processing

To filter out the systematic trends caused by effects such as changes in seeing which may cause the spurious detection of variable stars, we pass the light curves to a final post-processing module of the pipeline, where the Tamuz post-calibration algorithm (Tamuz et al. 2005) was applied. We de-trend all images by running Tamuz algorithm for a maximum of two times, as we found that more than this starts to noticeably degrade signals and may remove genuine variability. Fig. 3 shows the rms as a function of the mean instrumental magnitude for ‘raw’ light curves and light curves after two cycles of post-processing. The rms frame-to-frame scatter of the instrumental magnitude is a good indicator of the accuracy of the photometry. In addition, stars with a large dispersion for a given magnitude are, in principle, good variable candidates. However, it is possible that a light curve has a large rms due to bad measurements in some images, in which case the variability is spurious.

### 2.4. Caveats of DIA

We have found two features of the differential image construction with DanDIA that can impede photometry of some objects. Firstly, as noted by Bramich et al. (2011), due to the saturation effects on the RF, DanDIA discounts the area in the difference image that encompasses the saturated star and its immediate neighborhood. The convolution kernel on the RF is modelled as a circular pixel array of radius equal to twice the PSF FWHM in the current registered image. Consequently, stars in the neighborhood of saturated stars may suffer from imprecise photometry, missing photometric measurements, or it may have been impossible to extract any photometric measurements at all for such stars. We have reduced the exposure time as much as it is possible without degrading the S/N

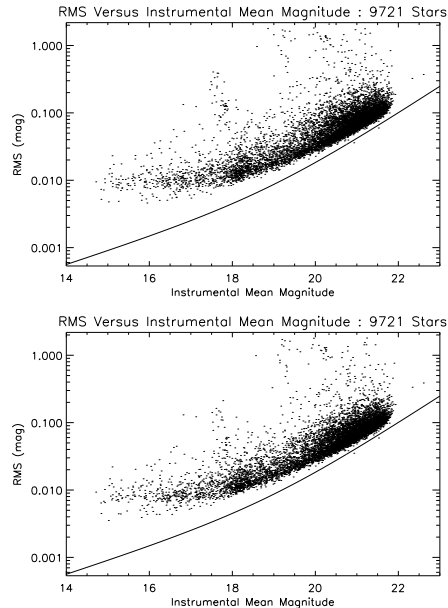


Fig. 3.— *Top*: Plot of rms vs mean instrumental  $r$  magnitude for each of the 9721 ‘raw’ light curves. *Bottom*: Plot of rms vs mean instrumental  $r$  magnitude for each of the 9721 ‘post-processed’ light curves. It is seen that there are fewer stars with large rms in the bottom plot compared to the top plot, and more stars with rms < 1% in the bottom plot than in the top one.

ratio to minimize the number of saturated stars. However, our RF still contains several saturated stars, which has affected the photometry of nearby variables. We do not consider candidate variables which are closer than 10 pixels to such stars.

Second, at the stage of variable selection, we found that a large number of stars had nearly identical light curve variation which was correlated in time. In many cases this false variability was correlated with the intra-night changes in PSF. In the top panel of Figure 4 we display the changes of the FWHM (in pixels) of the four photometric standard stars (Stetson 2000) located at different positions on the CCD.

We traced the origin of this effect to the combination of intra-night changes of the stellar PSF and the way DIA works. It is possible that this variability is induced at the subtraction stage of the DanDIA pipeline. When DanDIA convolves

the RF with other frames, it uses different parameters for each subregion (Sec. 2.2) of the grid. It is possible that at the edges of these subregions DanDIA finds it difficult to fit the convolution parameters. For stars in those areas, the intra-night PSF changes mean that any consistently inadequate convolution may show up as photometric variability. We had re-run the subtraction stage of the pipeline with the coarser grid of  $3 \times 3$  subregions and found induced changes in the light curves of some stars. For example, star *V81* reported by DK, was found by us to be non-variable on the initial run of the pipeline (Fig. 4, *Middle panel*, and Sec. 3.2). On the re-run, it started exhibiting a spurious variability of the type mentioned above, which is clearly seen in Fig. 4, *Bottom panel*. It is possible that during the re-run, this star turned out to be on the edge of the subregion while previously it was away from it. It is difficult to determine in advance false variability due to this effect, thus we have rejected such light curves through a visual examination of variable candidates.

## 2.5. Astrometry

The astrometric transformation between pixels and celestial coordinates for the RF was done using 46 photometric standard stars in the field of M53, taken from P. Stetson’s online catalogue (Stetson 2000) at Canadian Astronomical Data Center (CADC)<sup>2</sup>, which were uniformly distributed around the cluster centre and located sufficiently outside the cluster core. Since our observations were performed at a current epoch of J2010.235873, we first precessed the coordinates of these standards from J2000.0 epoch to the epoch of our observation (using IRAF utility *precess*), calculated the transformation solution from pixel to equatorial coordinates ( $\alpha, \delta$ ) and then precessed the solution back to epoch J2000.0. The standard deviations in the residuals of the coordinate transformation were  $0''.052$  and  $0''.053$  in right ascension and declination, respectively. We have found that in 10 years (from J2000.0 to J2010.225873), the cluster has moved by  $470''.2$  ( $450''.57$  in  $\alpha$  and  $-194''.59$  in  $\delta$ ). This is more or less consistent with the precession value of 1 degree per 72 years

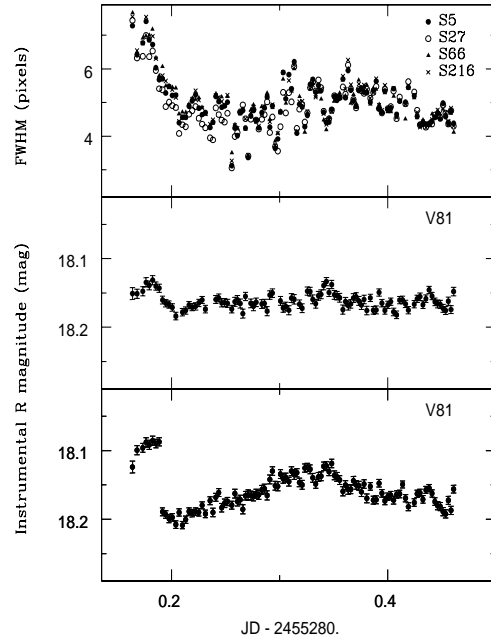


Fig. 4.— *Top panel*: Changes of the FWHM of four Stetson’s (2001) standard stars, *S5*, *S27*, *S66*, *S216*, with *R* magnitudes of 13.9, 14.5, 17.3 and 16.3 mag, respectively. *Middle and low panels*: the light curves of a star *V81*, obtained on running DanDIA subtraction module with  $6 \times 6$  and  $3 \times 3$  subdivision grid, respectively.

( $50''/\text{yr}$ ). The cluster’s proper motion was estimated earlier to be very small of  $\sim 0.5 \pm 1$  mas/yr (Dinescu et al. 1999).

## 2.6. Photometric Calibration

The absolute photometric calibration was obtained by using local secondary standards in M53. The instrumental *r* magnitudes were converted to the *R* standard system by using 26 selected photometric standard stars in the field of M53 from the Stetson’s online catalogue. The *R* magnitudes for these stars were obtained from the online USNO-A2.0 Catalogue Server (<http://archive.eso.org/skycat/servers/usnoa>).

The photometric transformation equation has the fitted form

<sup>2</sup>The catalogue is available at <http://www3.cadc-ccda.hia-ihp.nrc-cnrc.gc.ca/community/STETSON/standards/>  
 $r_{\text{std}} = 0.925(\pm 0.049)r_{\text{inst}} + 0.514(\pm 0.830)$ , (3)

where  $R_{\text{std}}$  is the standard magnitude and  $r_{\text{inst}}$  is the instrumental magnitude. The linear correlation coefficient is  $R = 0.967$ . The linear least square fit shown in Fig. 5 was used to obtain the standard  $R$  magnitudes of new variables found in this study.

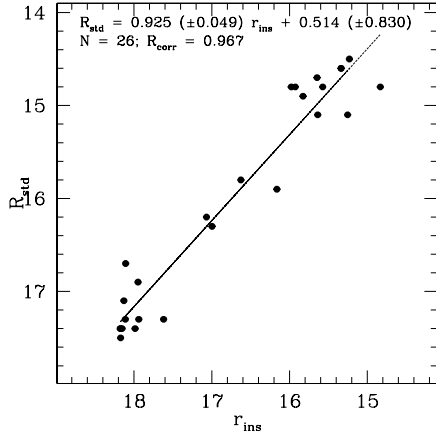


Fig. 5.— The transformation relationship between the instrumental  $r_{\text{inst}}$  and the standard  $R$  magnitudes obtained using 26 secondary photometric standard stars in M53.

### 3. Variable stars in M53

According to the updated 2010 online version of catalogue by C. Clement et al. (2001)<sup>3</sup> there are 90 variables in the field of M53. We have recovered the light curves of 64 of them. Out of 26 known variables which we could not recover, 12 were outside our field of view, 13 were saturated on our RF and one was at the edge of the CCD. In Table 1, we list the obtained equatorial coordinates (J2000.0) of the known variables recovered in our study, their offsets to the coordinates given by Clement et al. (2001) and their 2MASS identifications, if any. The offsets were calculated using

$$r'' = \arccos \left[ \sin \delta_1 \sin \delta_2 \cos (\alpha_1 - \alpha_2) + \cos \delta_1 \cos \delta_2 \right], \quad (4)$$

where  $(\alpha_1, \delta_1)$  and  $(\alpha_2, \delta_2)$  are right ascensions and declinations of the stars for which the offset is to be

calculated. We also provide the equatorial coordinates for variables from  $V61$  to  $V70$  which are not given in the Clement's catalogue. Several cases in Table 1 deserve special notes and are described in the text.

<sup>3</sup>A full updatable catalogue is accessible at <http://www.astro.utoronto.ca/people.html>

TABLE 1

REVISED EQUATORIAL COORDINATES OF IDENTIFIED KNOWN VARIABLES IN M53 AND THEIR OFFSETS WITH THOSE GIVEN IN THE CATALOGUE BY CLEMENT ET AL (2001).

ID	$\alpha(2000)$ (h:m:s)	$\delta(2000)$ ( $^{\circ}$ : $'$ : $''$ )	Offset ''	2MASS ID #	Notes/Remarks
V1	13:12:56.34	18:07:13.8	0.823	J13125634+1807139	
V2	13:12:50.27	18:07:00.8	0.511	J13125028+1807007	
V3	13:12:51.37	18:07:45.4	0.688	J13125132+1807461	
V4	13:12:43.88	18:07:26.2	0.559	J13124390+1807259	
V5	13:12:39.09	18:05:42.6	0.349	J13123907+1805424	
V6	13:13:03.90	18:10:20.1	0.541	J13130390+1810202	
V7	13:13:00.85	18:11:30.0	0.609	J13130086+1811302	
V8	13:13:00.42	18:11:05.1	0.615	J13130043+1811049	
V9	13:13:00.07	18:09:25.1	0.639	J13130013+1809256	
V10	13:12:45.72	18:10:55.5	0.467	J13124572+1810554	
V11	13:12:45.37	18:09:01.9	0.583	J13124540+1809020	
V15	13:13:12.374	18:13:55.6	0.500	-	
V16	13:12:46.19	18:06:39.1	0.541	J13124620+1806387	
V17	13:12:40.34	18:11:54.1	0.418	J13124030+1811540	
V18	13:12:48.67	18:10:13.1	0.590	J13124868+1810128	
V19	13:13:07.00	18:09:26.3	0.559	J13130702+1809262	
V22	13:12:51.97	18:05:16.7	0.327	J13125197+1805165	
V23	13:13:02.33	18:08:36.1	0.443	J13130235+1808359	
V24	13:12:47.28	18:09:32.3	0.566	-	
V25	13:13:04.40	18:10:37.3	0.664	J13130441+1810372	
V27	13:12:41.42	18:07:23.7	0.541	J13124143+1807235	
V29	13:13:04.26	18:08:47.0	0.443	J13130426+1808468	
V31	13:12:59.56	18:10:04.9	0.535	J13125960+1810046	
V32	13:12:47.72	18:08:35.8	0.488	J13124774+1808358	
V33	13:12:43.89	18:10:12.1	1.416	-	see individual notes
V34	13:12:45.70	18:06:26.0	0.566	J13124569+1806258	
V35	13:13:02.41	18:12:37.9	0.464	J13130235+1812373	
V36	13:13:03.28	18:15:10.5	0.535	J13130329+1815109	
V37	13:12:52.28	18:11:05.3	0.492	J13125227+1811050	
V38	13:12:57.14	18:07:40.5	0.727	J13125713+1807404	
V39	13:12:38.74	18:13:31.3	0.516	J13123874+1813312	
V40	13:12:55.85	18:11:54.8	0.535	J13125583+1811545	
V41	13:12:56.75	18:11:08.5	0.630	J13125679+1811093	
V42	13:12:50.55	18:10:20.0	0.395	J13125058+1810195	
V43	13:12:53.08	18:10:55.4	0.511	J13125306+1810552	
V44	13:12:51.66	18:10:00.5	0.590	-	
V45	13:12:55.15	18:09:27.4	0.590	J13125517+1809274	
V46	13:12:54.53	18:10:37.1	0.418	-	
V47	13:12:50.41	18:12:24.7	0.492	J13125043+1812246	
V51	13:12:57.58	18:10:49.6	0.549	-	



### 3.1. Variable stars with periods $P > 0.1$ days

Though we have obtained light curves for most of previously detected variables in this period range, we would not like to make conclusions regarding their variability due to the short span of our observations. However, several stars in this period range deserve special mention.

#### 3.1.1. Notes on individual variables

##### *V33*

Both Clement's (obtained from Evstigneeva et al. 1997) and our coordinates do not match with the position of this variable as marked in Kopacki (2000) ID chart. However, it is situated very close to a very bright secondary standard star  $S_4$  that is nearly saturated on our RF, which may account for the shift in the light centroid in our case.

##### *V52-V53*

These two stars separated by  $\sim 2''$  and DK reported that they could not resolve them. However, *V52* is clearly resolved on our images and its coordinates coincide with the coordinates given by Clement et al. (2001) with  $0.''3$  offset. Though we could not determine its period, its light curve shows the RRlab-type variability. At the position of *V53*, given by Kopacki (2000), there are 3 stars, one of which does show some variability; however its independent variability is under question. 2MASS position for *V53* is between these three stars.

##### *V57*

The coordinates of a star, identified by Kopacki (2000) as *V57*, do not match with the coordinates given by Evstigneeva et al. (1997). Coordinates of Evstigneeva et al. (1997) match another, fainter, star close to it. To investigate further, we have checked both stars, marked *V57\_1* and *V57\_2*, respectively, for variability. The star identified by Kopacki as *V57* (our *V57\_1*) does not show any variability, though with the listed period of  $P = 0.5683$  days, its light curve should have shown some variation over our 7.5 hrs of observations. Whereas the star that matches with Evstigneeva's

coordinates (our *V57\_2*) shows very clear variability with possible two pulsation periods of different amplitudes. Due to the limited time span of our observations, we could not determine its period, but the presence of Blazhko effect can be suspected from the observed light curve. Thus, we conclude that the star identified and marked on the ID chart by Kopacki (2000) as *V57* is a mis-identification, and the correct coordinates are given in Evstigneeva et al. (1997). Interestingly, there is one more star within this field, marked as *V57\_3*, which shows complicated variability of  $\sim 0.2$  d and a small amplitude of  $\Delta m \sim 0.11^m$ . In see Fig. 6 we show all three stars, marked accordingly, and their time-domain light curves. When we cross-correlated our list of known variables with the BSS catalogue by Beccari et al. (2008) (see Sec. 4.7), we have found a match of *V57* with the BSS #102387 from HST/WFPC2/PC sample to within  $0''.6$ . Since *V57* was identified as a RR Lyrae previously (for ex., Kopacki 2000), it is possible that it is *V57\_3* that is the BSS identified by Beccari et al. (2008). More work on a identification is in progress and the result will be reported in the forthcoming paper.

##### *V61-V70*

For these stars the updated 2010 online version of catalogue by Clement et al. (2001) does not provide equatorial coordinates. We have determined the coordinates of all of these stars and matched them to the 2MASS catalogue (Table 2). For *V61* DK did not provide the light curve as they stated that this star is merged with the long-period variable *V49* on their images. However, it shall be noted that variable *V49* (2MASS ID# J13125915+1814356) is a star well outside the cluster core at a distance of  $4'.54$  from the cluster centre, while *V61* is well inside the core at only  $1''.8$  from the centre; thus there is some mistake in their identification.

We shall note that for variables *V62*, *V63* and *V64* three sets of coordinates are available: from the online catalogue by Samus et al. (2009)<sup>4</sup>, de-

<sup>4</sup>The full catalogue is available at <http://vizier.cfa.harvard.edu/viz-bin/VizieR?-source=J/PASP/121/1378>. However, there is a mistake in the online catalogue star listing — the coordinates of a variable *V46* are lost, instead the coordinates of *V47* are assigned to it, and this mistake

TABLE 1—*Continued*

ID	$\alpha(2000)$ (h:m:s)	$\delta(2000)$ ( $^{\circ}$ :':")	Offset "	2MASS ID #	Notes/Remarks
V52	13:12:55.91	18:10:37.0	0.327	-	see individual notes
V53	13:12:55.78	18:10:36.0	0.615	J13125580+1810360	see individual notes
V54	13:12:54.29	18:10:31.5	0.590	-	
V55	13:12:53.45	18:10:36.6	0.492	-	
V56	13:12:53.69	18:09:26.0	0.590	-	
V57	13:12:55.44	18:09:57.9	1.699	J13125547+1809577	BSS, see individual notes
V58	13:12:55.59	18:09:31.0	0.492	-	
V59	13:12:56.67	18:09:20.8	0.441	-	
V60	13:12:56.99	18:09:36.5	0.418	J13125695+1809357	
V61-V70					see individual notes
V72	13:12:55.942	18:09:52.12	2.522		see individual notes
V73	13:13:03.34	18:09:25.1	0.655	-	
V74	13:12:49.68	18:07:25.9	0.427	-	BSS, Beccari et al. (2008)
V75	13:13:09.39	18:09:39.7	0.792	-	BSS, first report
V76	13:13:04.97	18:08:35.8	0.658	-	BSS, Beccari et al. (2008)
V79	13:12:46.60	18:11:36.7	0.148	-	BSS, DK
V80	13:12:57.46	18:10:14.8	1.294	-	see individual notes
V81	13:13:02.69	18:06:29.7	0.283	J13130271+1806294	
V82	13:12:56.44	18:13:09.9	0.850	-	
V83	13:12:50.11	18:07:43.0	0.187	-	
V87	13:13:01.92	18:10:13.2	0.475	-	BSS, first report
V89	13:13:08.15	18:07:38.4	0.884	-	BSS, first report

NOTE.—The coordinates listed above for all variables numbered up to *V60* are from Evstigneeva et al. (1997). Coordinates for *V73*–*V76*, *V87* and *V89* are from Jeon et al. (2003); for variables *V79*–*V83* from DK.

rived from 2MASS catalogue (probably precessed from J2000.0 to J2000.343), DK's and ours. For *V62*, Samus et al. (2009) give a position between *V62* and a star to the north from it with  $0''.535$  offset, while DK's and our coordinates coincide within  $0''.12$  with its position. *V63* has no 2MASS match; Samus et al. (2009) and our coordinates match within  $0''.02$ , but DK coordinates are off by  $2''.44$  and actually mark a different, non-varying star. For *V64*, Samus et al. (2009) use 2MASS coordinates (at J2000.343 epoch), but these give a position shifted by  $0''.374$  to the left, and DK miss the position by  $1''.215$ . The remaining variables, *V65* to *V70*, match perfectly with 2MASS sources. *V65* is a Stetson's (2000) secondary standard star *S67* (see Sec. 3.3).

### *V72*

We did not find any variability of the star that matches the coordinates given by DK. Though *V72* is situated in the heavily crowded core, we have clearly identified five stars within  $2''.75$  radius of the coordinates given by DK. The star which is variable according to DK is marked as *V72\_1*, the rest as *V72\_2*, *V72\_3*, *V72\_4* and *V72\_5*, respectively. While four of them do not show obvious variability, the star *V72\_2* is clearly varying with an estimated period of 0.12710 days and an amplitude of  $\sim 0^m.1175$ . We conclude that it is the star *V72* identified by DK, and that the period reported by them  $P_{DK} = 0.2542$  days is a multiple of the true period. The coordinates of *V72\_2* and its offset from DK coordinates are given in Table 1. In Fig. 7 we show the  $6''.5 \times 6''.5$  field around the coordinates given by DK, phase plot of *V72\_2* and time-domain light curves of these two stars.

### 3.2. Variables with periods $P < 0.1$ days

There are 15 short-period variable (SPV) stars of SX Phe type reported so far in M53. From our observations we were able to recover 11 of those stars. Three stars *V77*, *V88* and *V90*, were out of our FOV and one, *V78*, was saturated on our RF. For these 11 stars we have obtained the light curves and determined the periods. In several cases we have revised the periods given pre-

viously in the literature. In Table 3, we list these stars along with the previously reported periods, new periods and the average *R*-band magnitudes determined in this work.

### *V80*

At coordinates given by DK there is no star. However, within the circle radius  $3''.184$  of this location there are 7 stars clearly seen on our RF. This image region is shown in Fig. 8 with 7 stars marked on it. We have run the periodicity check (see details in Sec. 4.3) on the light curves of all of these stars. Three of them, *V80\_1*, *V80\_5* and *V80\_7*, show short-term variability and their light curves are shown in Fig. 8. Of these, *V80\_1* and *V80\_5*, show similar light curves and periods characteristic of SX Phe stars, but *V80\_5* has much larger variation amplitude of  $\Delta m = 0.9$  compared with  $\Delta m = 0.2$  of *V80\_1*. The light curve of a variable *V80\_7* is noisy with an amplitude of  $\Delta m \approx 0.6$ . It shall be noted that DK could not have determined the exact position of *V80* as they reported that this particular field was heavily crowded or blended on their RF. By comparing the light curves of their *V80* and our candidates, we conclude that the most probable match is candidate *V80\_1* (it has the same symmetric sinusoidal curve). The other two candidates, *V80\_5* and *V80\_7*, thus constitute new variables. Details on *V80\_5* are presented in Table 6, where it is assigned a name *SX25*, and on *V80\_7* in Table 9.

### *V81*, *V82*, *V83*

These three stars were first reported by DK as SX Phe stars. *V81* star is clearly resolved on our RF and has a 2MASS match. However, we find it non-variable. DK have reported that its variability is of either unknown type or that it was blended with a nearby suspected BSS, identified by them with USNO star B1.0 1081-0245846. However, USNO coordinates are located between *V81* and two nearby faint stars which do not show any variability. Stars *V82* and *V83* are also clearly resolved on our RF and also do not show variability of the type reported by DK (see Fig. 9). The results of the variability criteria (details are in Sec. 4.4) shown in Table 4 also indicate that these three stars are most probably not variable.

---

carries on till the end of the catalogue.

TABLE 2  
EQUATORIAL COORDINATES ( $\alpha, \delta$ ) OF KNOWN VARIABLES *V61-V70*.

ID	$\alpha(2000)$ (h:m:s)	$\delta(2000)$ ( $^{\circ}$ : ' : ")	2MASS ID #(J2000.0)	Note
V61	13:12:55.214	18:10:10.31	J13125521+1810103	
V62	13:12:53.995	18:10:29.81	J13125400+1810302	
V63	13:12:56.300	18:10:00.75	-	
V64	13:12:52.515	18:10:12.54	J13125254+1810125	
V65	13:13:04.669	18:10:59.44	J13130467+1810594	$\equiv$ S67
V66	13:13:01.578	18:10:03.90	J13130157+1810039	
V67	13:13:01.024	18:10:09.50	J13130102+1810095	
V68	13:12:56.577	18:08:23.13	J13125657+1808231	
V69	13:12:55.160	18:10:19.40	J13125616+1810194	
V70	13:12:55.320	18:09:42.00	J13125532+1809420	

TABLE 3  
REVISED PERIODS FOR PREVIOUSLY KNOWN SHORT-PERIOD VARIABLES IN M53. COLUMN (1) IS STAR'S ID BY CLEMENT ET AL. (2001) NOMENCLATURE, COLUMN (2) – PERIODS FROM THE LITERATURE, COLUMNS (3) AND (4) – NEW PERIODS AND STANDARD  $R$  MAGNITUDES FOUND IN THIS WORK.

ID	Period (days)	New period (days)	$\langle R \rangle$ (mag)	Note
V73	0.0701	0.071530	18.927	
V74	0.0454	0.045055	19.054	BSS
V75	0.0442	0.044178	19.455	BSS
V76	0.0415	0.041467	19.434	BSS
V79	0.0463	0.046255	19.183	BSS
V80	0.0674	0.065668	17.915	see individual notes
V81	0.0714	NV	17.310	see individual notes
V82	0.0221	NV	18.864	see individual notes
V83	0.1247	NV	18.749	see individual notes
V87	0.0479	0.046855	19.356	BSS
V89	0.0435	0.43278	19.435	BSS

NOTE.—Periods in the second column are from DK, except for the stars *V87* and *V89* where periods are from Jeon et al. (2003). NV stands for non-variable and BSS means that the star belongs to the BSS population.

TABLE 4

RESULTS OF THE VARIABILITY CRITERIA FOR STARS *V81*, *V82* AND *V83*.  $\mathcal{A}$  IS THE ALARM STATISTICS,  $\mathcal{F}$  IS THE SIGNIFICANCE LEVEL OF PERIODICITY FOUND, RMS IS THE STANDARD DEVIATION OF THE MEAN INSTRUMENTAL MAGNITUDE AND  $\sigma_{XS}$  IS THE EXCESS VARIANCE.

ID	$\mathcal{A}$	$\mathcal{F}$	rms	$\sigma_{XS}$
V81	2.7	$5.084 \times 10^{-3}$	0.01123	0.05233
V82	-0.09842	$7.49 \times 10^{-2}$	0.02073	0.07512
V83	0.45415	$7.044 \times 10^{-1}$	0.01923	0.08208

### 3.3. Standards as variables

Out of 192 secondary photometric standard stars known in M53 we have selected 43 for our

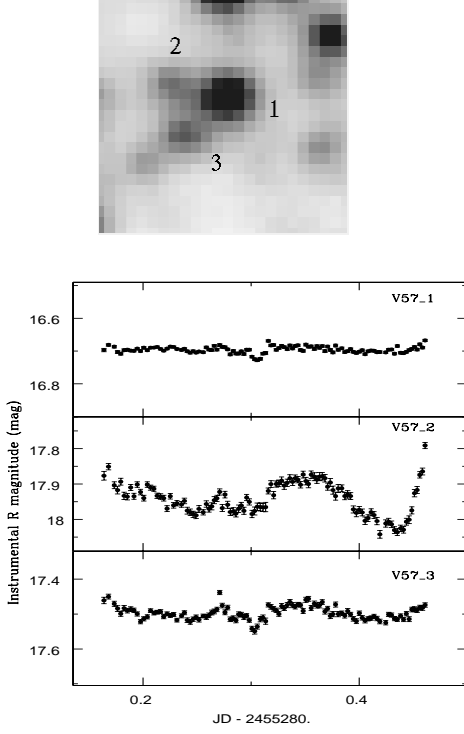


Fig. 6.—  $7'' \times 7''$  field around *V57* with marked stars and the light curves of *V57\_1*, *V57\_2* and *V57\_3*. The names of the stars are indicated on each panel.

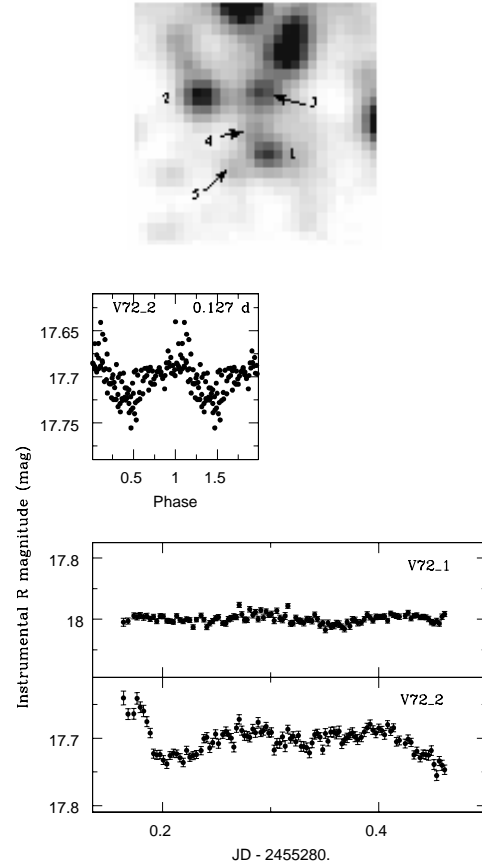


Fig. 7.—  $6.''5 \times 6.''5$  field around *V72* position as given by DK with marked stars, phase plot of *V72\_2* and light curves of *V72\_1* and *V72\_2* stars.

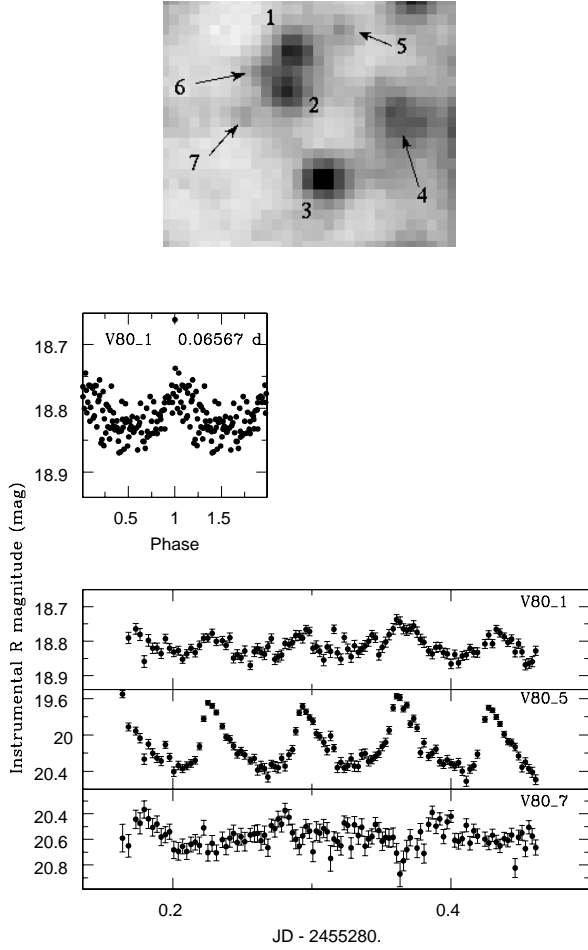


Fig. 8.—  $6.''5 \times 6.''5$  field around *V80* with marked stars, phase plot of *V80\_1* and light curves of *V80\_1*, *V80\_5* and *V80\_7* stars.

astrometric calibration (Sec. 2.5). However, when we tried to use these stars to devise the variable search criteria in this work, we found that some of the standard stars exhibit some sort of variability over the course of our 7.5 hrs of observations, ranging from slow variations in magnitude to sudden aperiodic changes. This is not the first time when standard stars in this cluster are found to be variable. Two variables discovered by DK, namely *V84* and *V85*, and identified by them as LPV with periods of 22.4 and 19.8 days, respectively, are in fact the secondary photometric standard stars *S1* and *S17* of Stetson (2000). One more variable star *V65* identified by Kopacki (2000) as SR type, although he couldn't determine its period, is in fact the standard star *S67* from Stetson (2000). We,

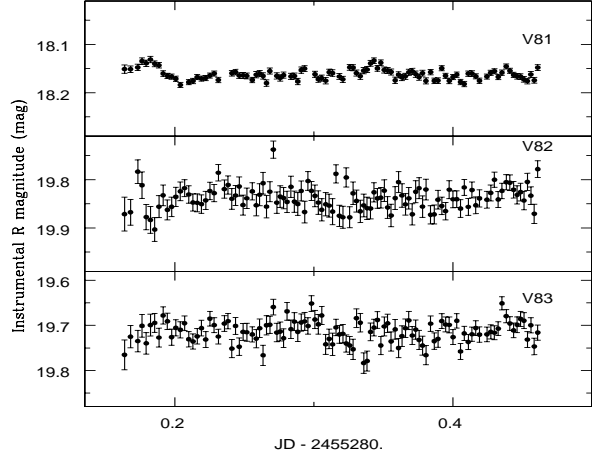


Fig. 9.— Light curves of *V81*, *V82* and *V83* stars.

however, could not confirm their variability as all three stars were saturated on our RF.

We have examined the variability in our set of selected standards. The properties of some of these stars are given in Table 5 and their light curves in Fig. 10. We noticed that several stars exhibit nearly identical variability and have concluded that this is the result of spurious, or induced, variability due to the combination of the intra-night PSF changes and DanDIA reduction procedure (see Sec. 2.4). Out of these, only *S65* shows different type of variability with  $\Delta m = 0.0413$  amplitude and is, most probably, a true variable (Fig. 11). It is interesting to note that star *S240*, apart from obviously induced variability, displays the possible signature of a EA-type eclipsing binary light curve. However, to determine the true light curve, this star has to be examined in greater detail. This will be done in a separate study.

#### 4. Detection of New Variables

The primary goal of our main survey is to identify possible microlensing events. We have used the commissioning data set to tune up and test our data reduction and analysis pipeline, without necessarily expecting to find new variable candidates in this data set. However, it is still useful to search for variability, since there is a chance of

TABLE 5

SOME OF THE STANDARDS FROM STETSON’S CATALOGUE (STETSON 2000) THAT EXHIBITED SPURIOUS VARIABILITY DURING OUR OBSERVATIONAL RUN. COLUMN (1) IS STAR’S ID BY STETSON (2000), (2) AND (3) ARE MEAN STANDARD  $R$  MAGNITUDES AND OBSERVED VARIATION, (4) IS THE DETERMINED PERIOD WHEN POSSIBLE. COLUMNS (5), (6) AND (7) ARE THE COMPUTED VARIABILITY STATISTICS (SEC. 4.4):  $\mathcal{A}$  IS THE ALARM STATISTICS,  $\mathcal{F}$  IS THE SIGNIFICANCE LEVEL OF PERIODICITY AND  $\sigma_{XS}$  IS THE EXCESS VARIANCE.

ID	$\langle R \rangle$ (mag)	$\Delta r$ (mag)	Period(d)	$\mathcal{F}$	$\mathcal{A}$	$\sigma_{XS}$
S65	17.121	0.042	0.2172	$1.0 \times 10^{-7}$	1.84	0.04
S70	15.567	0.182	spurious	$6.2 \times 10^{-10}$	16.9	0.22
S72	17.151	0.085	spurious	$6.4 \times 10^{-8}$	8.20	0.09
S74	17.338	0.157	spurious	$1.7 \times 10^{-8}$	3.83	0.10
S80	16.063	0.080	spurious	$8.1 \times 10^{-11}$	13.8	0.10
S230	15.427	0.050	spurious	$2.4 \times 10^{-10}$	11.9	0.07
S240	15.843	0.184	spurious	$1.5 \times 10^{-8}$	14.4	0.21

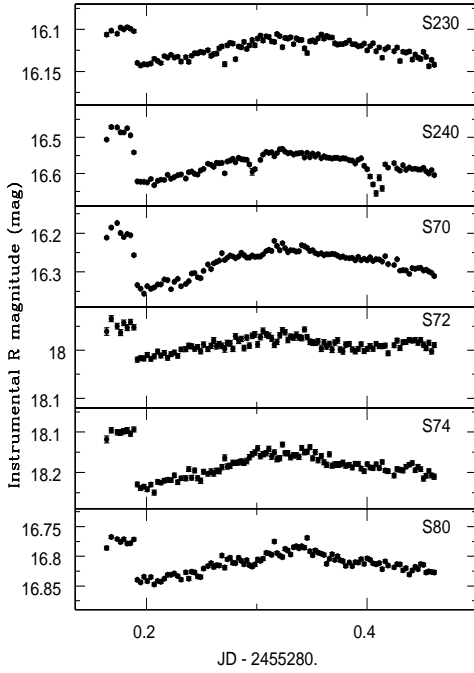


Fig. 10.— Light curves of standards suspected as variable.

discovery and the search can also yield interesting variable stars not found through earlier variable selection methods. Furthermore, we would expect to find false positives in the microlensing

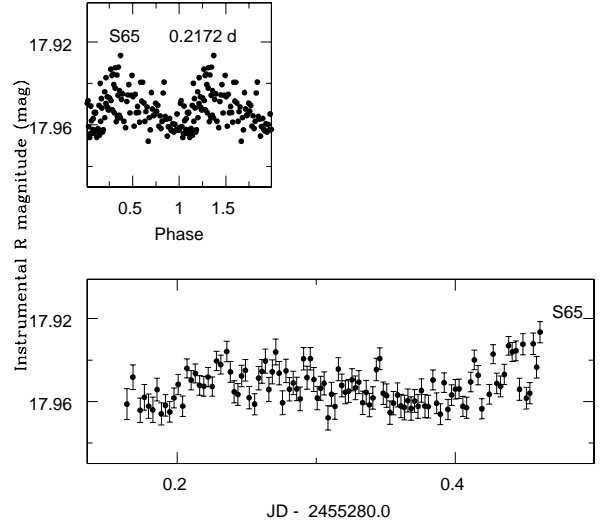


Fig. 11.— Phase and time-domain curves of the photometric standard star  $S65$ .

search — variables stars like dwarf novae, classic novae, etc (see Safonova & Stalin (2010) for discussion on contamination of ML searches). Finding these events and successfully identifying them

would demonstrate our ability to detect actual microlensing events in our data set in the future.

To search the data set of  $\sim 10,000$  light curves for variable stars, we take several main steps. Due to the large numbers, it is necessary to automate the detection of variable sources. We found that no single algorithm is appropriate for the detection of all kinds of variable stars present in our data, and that false positives (or missing variables) are high if we use just one algorithm. We thus implement several cuts to select promising candidates. In addition, we only consider light curves having more than 60 data points, since several variability detection algorithm can produce wrong results when significant amount of data is missing.

#### 4.1. Alarm Statistics

As a first algorithm, we have selected the alarm statistics from the VARTOOLS software package (Hartman et al. 2008). The ‘alarm’  $\mathcal{A}$  is defined as (Tamuz et al. 2006)

$$\mathcal{A} = \frac{1}{\chi^2} \sum_{i=1}^M \left( \frac{r_{i,1}}{\sigma_{i,1}} + \frac{r_{i,2}}{\sigma_{i,2}} + \dots + \frac{r_{i,k_i}}{\sigma_{i,k_i}} \right)^2 - \left( 1 + \frac{4}{\pi} \right), \quad (5)$$

where  $r_{i,j}$  is the residual of the  $j$ -th measurement of the  $i$ -th run and  $\sigma_{i,j}$  is its uncertainty. The sum is over all the measurements in a run and then over the  $M$  runs. A ‘run’ is defined as a maximal series of consecutive residuals (in the folded light curve) with the same sign. The  $\chi^2$  is the known function

$$\chi^2 = \sum_{i=1}^N \left( \frac{r_i}{\sigma_i} \right)^2, \quad (6)$$

where the sum is over  $N$  observations. In contrast to  $\chi^2$  itself,  $\mathcal{A}$  is not sensitive to a systematic overestimation or underestimation of the uncertainties. It is easy to see that  $\mathcal{A}$  is minimal when the residuals alternate between positive and negative values, and that long runs with large residuals increase its value. The minimal value of the summation is exactly  $\chi^2$ , and therefore the minimal value of  $\mathcal{A}$  is  $-4/\pi$ . We find that as an initial assessment, the alarm statistics is good for large sudden (aperiodic) variations, but that it fails in case of the short-period variability. It cannot easily distinguish between non-variability with large noise and very regular short periodicity, which we already noticed when we tried to use the ordinary

$\chi^2$ -statistics. However, even in detecting large variations, the alarm results have to be viewed with caution, as it picks up the false variability, like in case of systematic variations found in standard stars (see Sec. 3.3). We still found it useful, as high values of alarm statistics may indicate eclipsing binary, microlensing event or any non-periodic transient.

#### 4.2. Excess variance method

Any light curve of a variable star candidate varies due to measurement errors  $\sigma_i$  and intrinsic variations. The variance of such a light curve consisting of  $N$  data points with amplitude  $X_i$  is given by

$$S^2 = \frac{1}{N-1} \sum_{i=1}^N (X_i - \langle X \rangle)^2. \quad (7)$$

This measured variance has contributions from both intrinsic source variability and measurement uncertainty. Therefore to know if any intrinsic variations are present in the light curve, one needs to remove the contribution of measurement errors to the observed variance. The commonly used approach to get an idea of the intrinsic variation present in the candidate light curve is to use the ‘excess variance’ (Nandra et al. 1997; Vaughan et al. 2003), which is defined as

$$\sigma_{XS}^2 = S^2 - \sigma_{err}^2, \quad (8)$$

where  $\sigma_{err}^2$  is the average variance of the  $N$  measurements, given as

$$\langle \sigma_{err}^2 \rangle = \frac{1}{N} \sum_{i=1}^N \sigma_{err,i}^2. \quad (9)$$

A large value of  $\sigma_{XS}^2$ , much in excess of the measurement errors might hint for the presence of variations in the light curve.

#### 4.3. Lomb-Scargle Periodogram

The Lomb-Scargle (LS) periodogram (Lomb 1976) is an algorithm designed to pick out periodic variables in an unevenly sampled data. The periodogram statistic,  $\Theta$ , measures the fit for a given pulsation frequency. The probability distribution of  $\Theta$  is then used to calculate the probability,  $P(\Theta > c)$  of obtaining the value of the periodogram higher than the actual observed value,



$\Theta = c$ , from a hypothetical pure noise signal. An unlikely good fit, corresponding to small  $P$ , is interpreted as detection of the corresponding period. Its complement probability,  $\mathcal{F} = 1 - P(\Theta > c)$ , is called the significance level. Thus, the likelihood of the existence of a periodic signal can be established with the ‘false alarm probability’  $\mathcal{F}$  — a simple estimate of the significance of the height of a peak in the periodogram. A small value of  $\mathcal{F}$  indicates a highly significant periodic signal. We have used the implementation of this algorithm given in Press et al. (1992) and this seems to be a good criteria to pick periodic variability present in the dataset.

#### 4.4. Final Selection

For selecting candidate variable stars from the original light curve database, we used a combination of three algorithms described above, namely (a) alarm statistics, (b) excess variance and (c) Lomb periodogram. After applying these three algorithms to the sets of secondary photometric standards and variable stars known in M53 (total 114 stars), we have devised the following criteria for the final selection of variables from our list of  $\sim 9,700$  candidate variable stars,

$$\begin{cases} \mathcal{A} > 1.0; \\ \mathcal{F} < 10^{-4}; \\ \sigma_{XS} > 0.09; \\ \text{rms} > 0.01. \end{cases} \quad (10)$$

A total of 310 candidate variable stars were found to satisfy the criteria simultaneously. For these candidates, we calculated the periods using two algorithms: the Lomb periodogram and the Lafler & Kinman (1965) algorithm (LK). From the highest peak in the Lomb periodogram we detect the initial estimate of the period. This period is then passed on to LK algorithm. LK method provides a systematic approach to testing a series of trial periods (with an increment of 0.0001 days) and looking for the period that results in the “smoothest” phase curve. The  $N$  observed points are sorted by phase, and the sum of the squares of the difference in magnitude of successive pairs of points is used to rank the trial period. The smallest value of the figure of merit

$$\Theta = \sum_i (m_i - m_{i+1}) / \sum_i (m_i - \overline{M})^2, \quad (11)$$

where  $\overline{M} = m_i/N$  should be the nearest to the correct period since this represents the smallest successive changes in the light curve.

#### 4.5. False Positives

Finally, we visually inspect the light curves to remove false positives. We noticed that due to the intra-night changes of the PSF, several stars selected as variables by our selection criteria, have, in fact, variability induced by the same mechanism as was discussed in Sec. 2.4. This type of variability is easily detected by eye as it is virtually identical in such false light curves, and these stars were removed from the candidate list. We also noted that during our continuous observations of  $\sim 7.5$  hrs, the coordinates of the field centre drift between the images through the night. The typical intra-night drift was  $\sim 25$  pixels, but it had some effects in our data. The drift caused stars at the edges of the field to enter and exit the CCD’s field of view during the night, resulting in incomplete light curves for those stars. We remedied that by eliminating the strips of  $\sim 20$ -pixel width along the edges from our images. Finally, we reject any variable star that is less than 10 pixels away from a variable candidate and has higher rms in flux. This criterion enabled us to eliminate stars whose variability was induced by its proximity to a genuine variable.

#### 4.6. The Classification of New Variables

The basic characteristics of our observations and the achieved precision of the relative photometry allowed us to establish the fact of light variations in the variable star candidates. However, the total duration of our observations was not long enough for reliable classification of a large number of them. Nevertheless, the obtained light curves made it possible to tentatively estimate the type of some of the discovered variables from the shape and characteristic features of the light curves.

##### 4.6.1. Candidate SX Phe-type stars

We have found 22 stars whose light curves parameters, i.e. short periods and low amplitudes, allow us to classify them as potential SX Phe stars. SX Phe stars known in globular clusters usually have periods between 0.03 – 0.14 days and they often show multiple frequencies of light variations.

However, with our limited span of observations, it was very difficult to establish the complicated frequency patterns, so we aimed to find at least the main periodicity. The parameters of these candidates are listed in Table 6. For each star we provide designation, equatorial coordinates ( $\alpha, \delta$ ), period  $P$ , mean brightness in  $R$ , range of variability  $\Delta r$ , epoch of light-minimum  $T = JD - 2455280$  and in the Notes we present the BSS match, possible variability type, or pulsation mode as inferred from the  $P - L$  diagram.

Several methods are available to confirm the genuine nature of the SX Phe candidates. It is known that observational identification of the pulsational modes in SX Phe is difficult. McNamara (2000) and, subsequently Rodríguez & López-González (2000), suggested that at fundamental mode, SX Phe preferably show large amplitudes ( $> 0.2$ ) and asymmetric light curves. They also follow a tight relation between their fundamental mode period and luminosity ( $P - L$  relation). SX Phe are also the blue straggler stars found in a large number in globular clusters ( $\sim 200$  in this cluster, Beccari et al. 2008). Thus, a match between known BSS and our SX Phe candidates would argue in favour of their SX Phe nature (see Sec. 4.7).

Based on a study of 6 SX Phe stars in M53, Jeon et al. (2003) derived the following  $P - L$  relation for the fundamental mode

$$\langle V \rangle = -3.01(\pm 0.262) \log P + 15.31(\pm 0.048). \quad (12)$$

We have used our derived periods and  $R$  magnitudes for 7 previously known SX Phe stars ( $V73$ ,  $V74$ ,  $V75$ ,  $V76$ ,  $V87$ ,  $V89$  from Jeon et al. (2003) and  $V79$  from DK) and 6 new SX Phe candidates that have BSS matches (except  $SX9$ ,  $SX9_1$ ,  $SX6$  and  $SX17$ , see the discussion later in this subsection) to derive the  $P - L$  relation. Our relation is surprisingly nearly identical to that of Jeon et al. (2003),

$$\langle R \rangle = -3.019(\pm 0.382) \log P + 15.300(\pm 0.501). \quad (13)$$

In Figure 12, we display the period and mean  $R$  magnitude relation for 7 known SX Phe stars and 22 new SX Phe candidates in M53. We note that variable  $V74$  was found by Jeon et al. (2003) to lie far away from the  $P - L$  line; this is possibly due to the wrong period reported by the authors in their Fig. 7. Besides, the authors excluded this vari-

able from the fundamental  $P - L$  fitting suggesting that it was in a higher pulsational mode. However, if it is in the first harmonic mode, its period can be converted to the fundamental mode by the theoretical relation  $P_{1H}/P_F = 0.783$  (Jeon et al. 2004). Once corrected for that, we can see that  $V74$  lies on the  $P - L$  line together with other SX Phe stars (see Fig. 12). In our sample of SX Phe candidates we have two stars which have similar periods but different magnitudes (variables  $SX9_1$  and  $SX_9$  in Table 6). It is possible that only one of them is variable and another has variability induced by its proximity. By the selection criteria adopted in Sec. 4.5, we choose the star which has smaller rms in flux to be genuinely variable; thus, we select the star  $SX9_1$ . This star lies above the fundamental mode  $P - L$  line; when we convert its period by using the same relation  $P_{1H}/P_F = 0.783$  (Jeon et al. 2004), it falls close to that line. Stars with converted periods,  $SX9_1$  and  $V74$ , are marked by circles in the Figure 12.

The stars that fall along the  $P - L$  relation can be considered with high probability, given also their periods and shape of light curves, as belonging to the SX Phe type. Stars in the top left quadrant of the plot (variables  $SX6$ ,  $SX16$ ,  $SX17$ ,  $SX24$ ) are presumably in a higher pulsational mode. They also have smaller amplitudes (0.1606 on average) comparing to the ones pulsating presumably in fundamental mode (0.4365 on average). We have derived the least square fit for them and found that it is nearly parallel to the fundamental mode fit,

$$\langle R \rangle = -2.740(\pm 1.160) \log P + 14.371(\pm 1.600). \quad (14)$$

Stars that are located to the right and below the fundamental  $P - L$  line though undoubtedly variable (see their light curves in Fig. 13), are most probably not SX Phe type. Stars  $SX7$  and  $SX20$  are possibly RR Lyrae, while others ( $SX12$ ,  $SX13$ ,  $SX15$ ,  $SX23$ ) are of uncertain type. But since their periods exceed 0.1 days, we cannot truly determine their nature. We thus confirm SX Phe-type fundamental mode pulsations for 11 new variables (namely,  $SX2$ ,  $SX3$ ,  $SX4$ ,  $SX5$ ,  $SX8$ ,  $SX10$ ,  $SX11$ ,  $SX14$ ,  $SX21$ ,  $SX22$ ,  $SX25$ ) and probable higher pulsational mode for 5 new variables:  $SX6$ ,  $SX9_1$ ,  $SX16$ ,  $SX17$ ,  $SX24$ . The phase and time-domain light curves of all 22 stars are shown in Figure 13 and their parameters are given in Table 6. The po-

TABLE 6

EQUATORIAL COORDINATES AND LIGHT CURVE PARAMETERS FOR NEW SXPHE-TYPE CANDIDATES IN M53.  $\Delta r$  AND EPOCH WERE OBTAINED BY IRAF TASK *pdm*.

Variable designation	$\alpha(2000)$ h:m:s	$\delta(2000)$ ( $^{\circ}$ :':")	P (d)	$< R >$ (mag)	$\Delta r$ (mag)	epoch (d)	Note
SX2	13:12:48.29	18:13:18.7	0.039362	19.6018	0.2924	0.2039	SXPhe,F,BSS
SX3	13:12:48.27	18:14:34.5	0.059824	18.7855	0.16501	0.1763	SXPhe,F,BSS
SX4	13:12:48.69	18:10:10.2	0.049500	19.4494	0.41865	0.3733	SXPhe,F,BSS
SX5	13:12:48.70	18:10:11.3	0.050400	19.3330	0.38424	0.2634	SXPhe,F
SX6	13:12:49.91	18:08:56.5	0.044755	18.1171	0.16693	0.3482	SXPhe,1H,BSS
SX7	13:12:51.74	18:10:33.8	0.132701	19.6519	0.37991	0.2409	RR1?
SX8	13:12:52.03	18:09:53.6	0.099101	18.7416	0.37707	0.2517	SXPhe,F
SX9 <sub>1</sub> <sup>†</sup>	13:12:52.91	18:10:35.7	0.054056	18.5738	0.2819	0.216	SXPhe,BSS?
SX9 <sup>†</sup>	13:12:52.99	18:10:35.4	0.056756	19.6975	0.59367	0.216	BSS?
SX11	13:12:53.66	18:08:57.7	0.052932	19.3140	0.42881	0.2807	SXPhe,F
SX12	13:12:53.89	18:09:13.2	0.100001	19.4074	0.32196	0.3807	not SXPhe, uncertain
SX13	13:12:54.52	18:09:32.6	0.112712	19.4671	0.49331	0.3733	not SXPhe, uncertain
SX14	13:12:54.78	18:09:37.6	0.071130	18.6844	0.52035	0.3032	SXPhe,F,BSS
SX15	13:12:56.34	18:11:54.2	0.137101	20.4167	0.60844	0.3258	not SXPhe, RR1?
SX16	13:12:56.37	18:11:05.4	0.049900	17.9848	0.17625	0.1637	SXPhe,1H
SX17	13:12:57.17	18:09:41.9	0.040567	18.0077	0.13385	0.1824	SXPhe,1H,BSS
SX24	13:12:57.64	18:10:43.0	0.033724	18.4832	0.16544	0.3733	SXPhe,1H
SX19	13:12:58.30	18:08:41.3	0.044378	19.3035	0.33948	0.1637	SXPhe,F,BSS
SX20	13:12:59.53	18:09:17.5	0.134857	18.7493	0.16805	0.384	RR1?
SX21	13:12:59.51	18:11:17.4	0.037762	19.5682	0.26318	0.2983	SXPhe,F,BSS
SX22	13:13:01.92	18:12:30.4	0.045955	19.5604	0.38023	0.1824	SXPhe,F
SX23	13:13:04.21	18:10:59.4	0.107312	19.6818	0.38479	0.2039	not SXPhe, uncertain
SX25	13:12:57.37	18:10:15.3	0.066868	19.1302	0.96035	0.4111	$\equiv$ V80_5,SXPhe,F

NOTE.—<sup>†</sup> These two stars are separated by  $1''.2$  arcsec. Though their periods and epochs are nearly the same which would argue that there only one is variable, the amplitude of a fainter star is twice that of a brighter star. They also match within  $1''$  to a BSS (see Sec. 4.7), which coordinates (Beccari et al. 2008) are located exactly between these two stars. Their BSS nature is also under question, as Beccari et al. (2008) could not resolve them and thus must have used their combined light to derive their conclusion. More discussion is in the text.

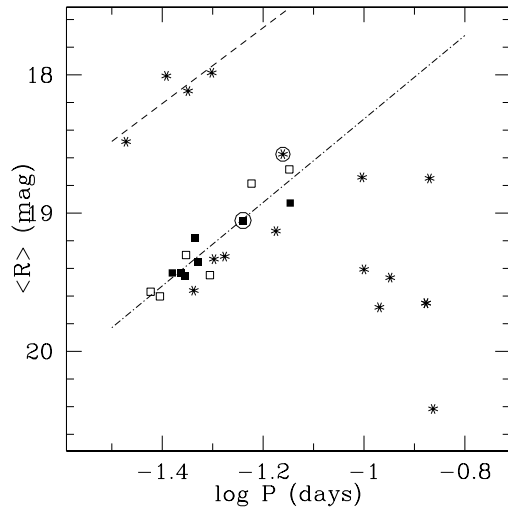


Fig. 12.— Mean  $R$  magnitude vs. period diagram. Squares represent stars used in the fundamental mode fitting; filled squares are previously known SX Phe in M53 and open squares are new SX Phe. Filled circled square is the star  $V74$  with the period converted from first harmonic to fundamental mode. Asterisks are remaining SX Phe candidates. Circled asterisk is an SX Phe candidate  $SX9\_1$  with the period converted to fundamental mode. Four top asterisks are most probably SX Phe in a higher pulsational mode and we have derived the linear fit for them.

sitions of 16 confirmed SX Phe stars on the CCD image are given in Figure 1.

Given the results of our study, the number of confirmed SX Phe stars in M53 reaches 28: 12 previously reported (with exclusion of  $V81$ ,  $V82$  and  $V83$ ) plus 16 discovered by us, and it is quite possible that there are much more yet undiscovered. SX Phe stars in globular clusters can have very short periods (down to 0.025 days) and very small amplitudes, for ex., 25% of 149 SX Phe stars in Rodríguez & López-González (2000) catalogue have amplitudes of  $< 0.^m05$ . Thus we cannot exclude the possibility that many of the apparently non-varying stars in the SX Phe region vary, but with undetectable by us amplitudes. More sensitive observations are necessary to search for this exciting class of variables.

#### 4.6.2. RR Lyrae Candidates

We tentatively classify the variable candidates with estimated periods of  $0.15 < P < 0.2$  days and a characteristic shape of a light curve as RR Lyrae variables (Clement et al. 2001). The light curves of these 14 RR Lyrae candidates are shown in Figure 14. The equatorial coordinates ( $\alpha$ ,  $\delta$ ) of these stars, mean brightness in  $R$ , rough estimate of the period, amplitude of variability  $\Delta r$ , the epoch of light-minimum ( $T = JD - 2455280$ ) and a possible variability type are given in Table 7. Their positions on the CCD image are given in Figure 2 *Top*.

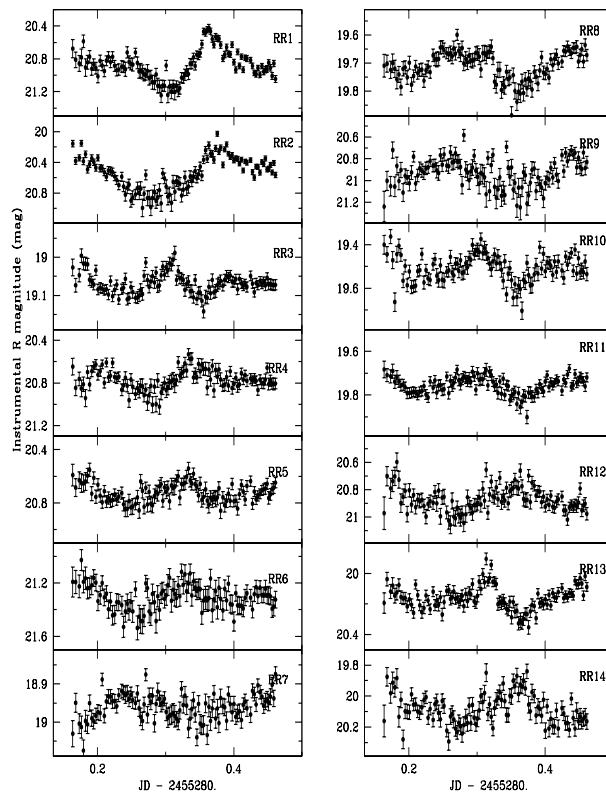


Fig. 14.— Time-domain light curves of RR Lyrae candidates.

#### 4.6.3. Eclipsing Binaries Candidates

Though about 14% of the nearly 200 BSS in this cluster are estimated to be in binary systems (Beccari et al. 2008), no eclipsing binary was ever

TABLE 7

EQUATORIAL COORDINATES AND LIGHT CURVE PARAMETERS FOR NEW RR LYRAE-TYPE STARS IN M53.  $\Delta r$  AND EPOCH WERE OBTAINED BY THE IRAF TASK *pdm*.

Variable designation	$\alpha(2000)$ (h:m:s)	$\delta(2000)$ ( $^{\circ}$ : ' : ")	$< R >$ (mag)	Period (d)	$\Delta r$ (mag)	epoch (d)	Remarks
RR1	13:12:45.40	18:09:04.1	19.809	0.071	0.82294	0.2933	RRab
RR2	13:12:48.74	18:10:12.7	19.524	0.5034	1.04199	0.2782	RRab
RR3	13:12:53.82	18:09:18.7	18.151	0.2924	0.15097	0.3556	RRc
RR4	13:12:54.03	18:09:11.4	19.720	0.071	0.48068	0.2909	RRc
RR5	13:13:01.33	18:10:15.9	19.682	0.5034	0.31814	0.3807	RRc
RR6	13:12:47.13	18:10:29.0	20.215	0.2924	0.48075	0.2382	RRc?
RR7	13:12:54.58	18:09:45.4	18.074	0.071	0.21463	0.1793	RRc?
RR8	13:12:45.18	18:11:22.4	18.739	0.5034	0.32282	0.3507	RRc
RR9	13:12:48.29	18:13:18.7	19.846	0.2924	0.84712	0.1637	RRc?
RR10	13:12:38.97	18:09:07.2	18.556	0.071	0.3408	0.3659	RRab?
RR11	13:12:45.18	18:11:22.4	18.788	0.5034	0.2573	0.3733	RRc
RR12	13:12:48.29	18:13:18.7	19.820	0.2924	0.46049	0.261	RRc
RR13	13:12:38.97	18:09:07.2	19.156	0.071	0.45296	0.3757	RRab
RR14	13:12:45.18	18:11:22.4	19.090	0.5034	0.45335	0.2585	RRc

NOTE.—The periods are derived from incomplete light curves and are only approximate due to the short span of our observations.

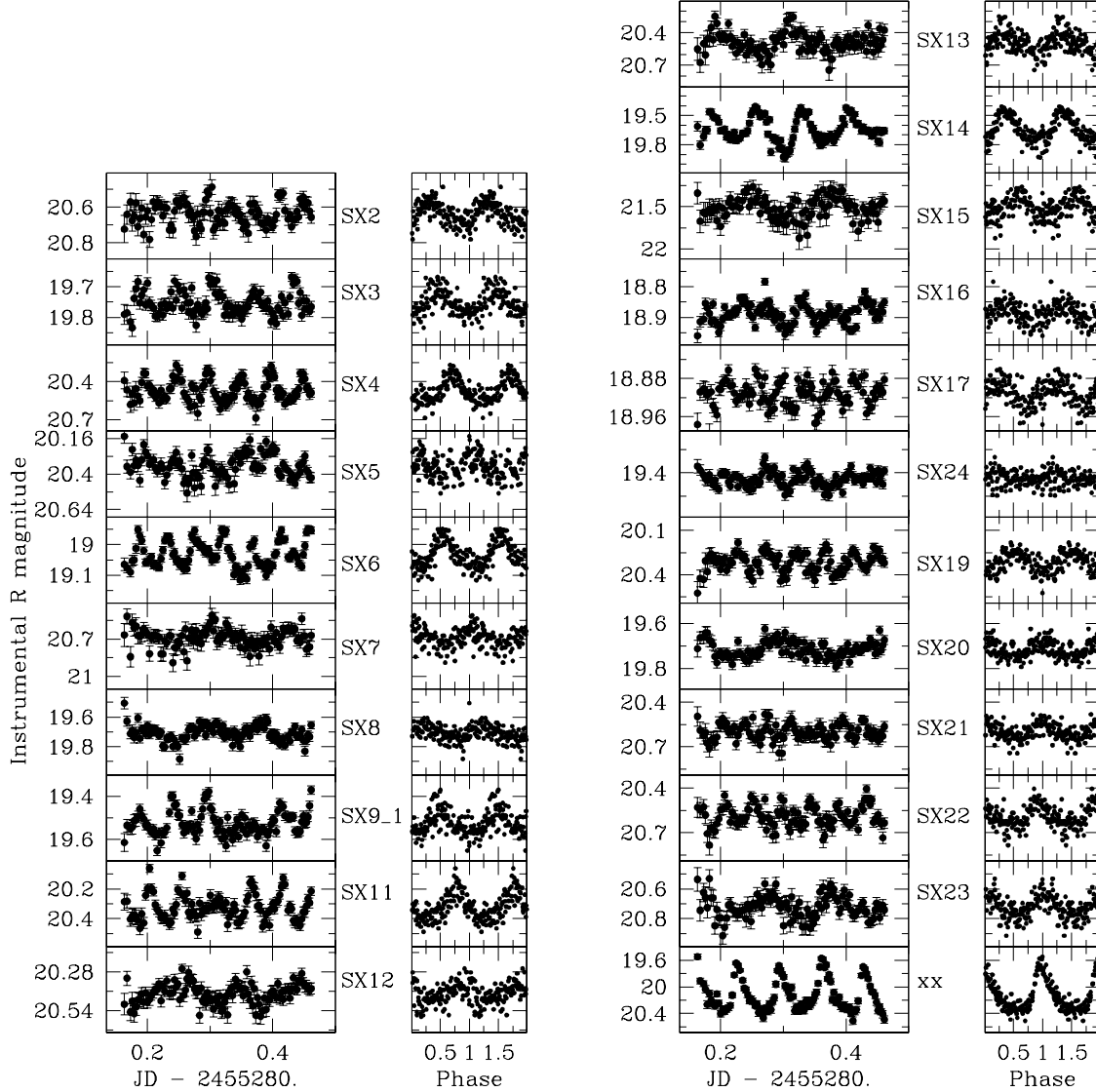


Fig. 13.— Phased and time-domain light curves of 22 SX Phe candidates from Table 6.

found. Here we report the discovery of 10 stars of W Ursa Majoris (W UMa) type and 2 detached eclipsing binaries. W UMa-type stars are contact binaries and it was noted (Kaluzny 1997) that almost all known eclipsing main-sequence binaries with periods shorter than about 0.4 days show EW-type light curves. All our suspected W UMa-

type candidates have periods of 0.1 d on average and indeed mostly display EW-type light curves. For each star we provide designation, equatorial coordinates  $(\alpha, \delta)$ , mean brightness in  $R$ , rough estimate of the period, range of variability  $\Delta r$ , epoch of light-minimum  $T = JD - 2455280$  and in the Notes we present a possible variability type or

BSS match. The phase and time-domain curves are presented in Figure 15. In Figure 16 we show the time-domain light curves of two long-period eclipses *E1* and *E3*, which can be either detached binaries or eclipsing Cataclysmic Variables (CV). The positions of these binaries on the CCD image are given in Figure 2.

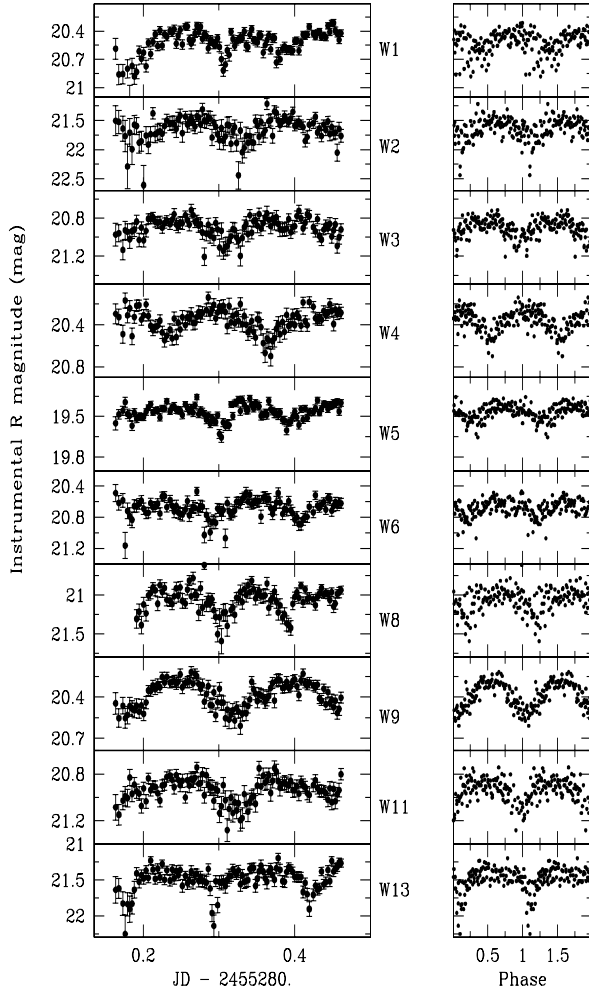


Fig. 15.— Phase and time-domain light curves of W UMa candidates.

#### 4.6.4. Unclassified Candidates

In addition to the unclassified variable candidates discussed previously in Sections 3.1.1, 3.2

and 4.6.1, we have found 28 more stars that show definite light variations, but which are also impossible to classify due to the short span of our observations and their possible long periods and irregular nature. Their variability, however, is undoubtful judging from their light curves (Figure 17). The equatorial coordinates and photometric parameters of these variables are presented in Table 9. Their positions on the CCD image are given in Figure 2. Several of these stars were matched to the BSS catalogue by Beccari et al. (2008) (Table 10). Star *VC23* is a possible long period variable (LPV), following the method described in Hartman et al. (2004) in which a star is defined as an LPV when a light curve can be fitted by a parabola. Also in Table 9 is given the data on *V57\_3* and *V80\_7*.

#### 4.7. Blue Stagglers in M53

We have cross-correlated the coordinates of the known and newly discovered variables with the BSS database of M53 by Beccari et al. 2008 (via private communication) and found 23 matches within 0.1 arcsec. Seven cases are matches with previously known variables, of which four, namely *V57*, *V75*, *V87* and *V89*, are reported by us for the first time (Table 1), and 16 are new. Out of them, ten are SX Phe stars, one is a W UMa candidate, one is a long-period eclipse and four are of uncertain type. All stars matched by us with BSS are shown in Table 10. For each star we provide BSS catalogue number by Beccari et al. (2008) nomenclature, our designation, mean *V* magnitude from BSS catalogue, mean brightness in *R* and period determined in this work, possible

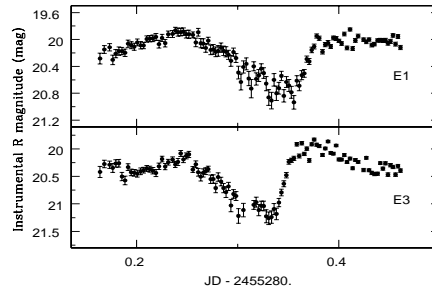


Fig. 16.— Light curves of long-period eclipses.

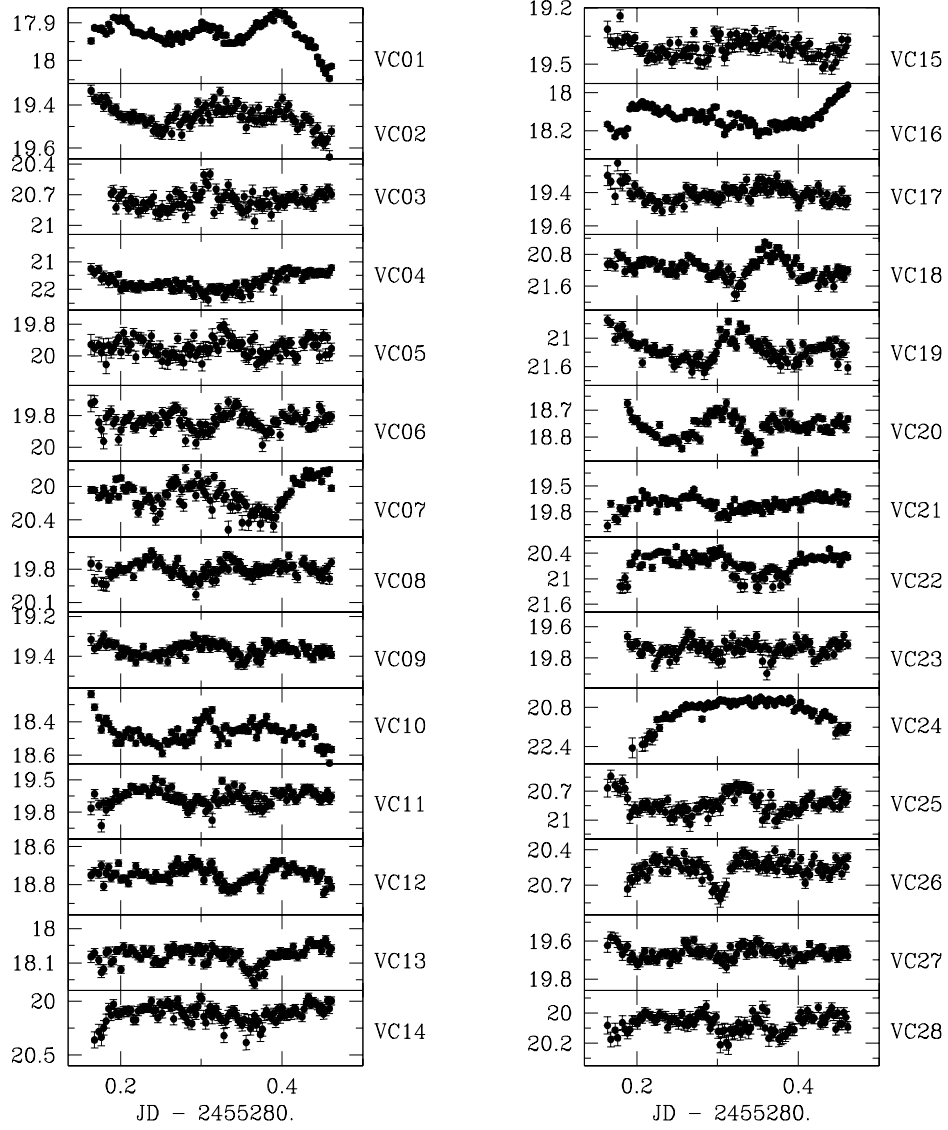


Fig. 17.— Light curves of uncertain type variables labelled with their designations as given in Table 9.



TABLE 8

EQUATORIAL COORDINATES AND LIGHT CURVE PARAMETERS FOR NEW CANDIDATE ECLIPSING BINARIES IN M53.  $\Delta r$  AND EPOCH WERE OBTAINED BY THE IRAF TASK *pdm*.

Variable designation	$\alpha(2000)$ (h:m:s)	$\delta(2000)$ ( $^{\circ}$ : ' : ")	Period (d)	$\langle R \rangle$ (mag)	$\Delta r$ (mag)	epoch (d)	Remarks
W1	13:12:43.70	18:10:09.0	0.063701	19.495	0.79939	0.1824	EW?
W2	13:12:51.07	18:11:11.9	0.152667	20.522	1.22333	0.3258	EW?
W3	13:12:51.41	18:09:37.4	0.039362	19.846	0.4898	0.2807	EW?
W4	13:12:53.98	18:09:49.0	0.063701	19.339	0.7531	0.3683	EW?
W5	13:12:53.21	18:09:47.3	0.152667	18.520	0.29791	0.3032	EW?
W6	13:12:57.46	18:10:29.6	0.039362	19.641	0.60217	0.3085	EW?
W8	13:12:56.66	18:08:18.7	0.063701	19.999	0.97774	0.3032	EW?
W9	13:12:59.00	18:10:21.9	0.152667	19.369	0.39071	0.3282	BSS, AH Vir?
W11	13:13:01.04	18:10:01.6	0.039362	19.881	0.53721	0.311	EW?
W13	13:13:11.43	18:10:34.2	0.063701	20.383	1.05576	0.1763	EW?
E1	13:12:55.07	18:09:27.9	0.21427	19.203	1.08425	0.3556	CV/EB?
E3	13:12:59.98	18:09:24.8	0.24482	19.439	1.81670	0.3085	BSS, EW/EB?

NOTE.—The periods are derived from incomplete light curves and are only approximate due to the short span of our observations.

variability type and in the Remarks we indicate who has first reported the match. The study in which these new BS stars are analyzed by combining both Beccari et al. (2008) and our catalogues is in progress.

## 5. Conclusion

We carried the all-night observation of the globular cluster NGC 5024 (M53) using 2-m *HCT* telescope of the Indian institute of Astrophysics, Hanle, India. As a result, we obtained 101 *R*-band images of the cluster. The reduction of our data using the pre-released version of the DanDIA pipeline (Bramich 2008) revealed significant short-term brightness variations in  $\sim 300$  stars. 79 of them are candidates for new variables, out of which 16 are SX Phe stars (our conclusion was based on the periods, shapes of light curves and analysis of  $P - L$  relation), 10 are W UMa-type eclipsing binaries (the conclusion is based on the shapes of the light curves), 14 are RR Lyrae candidates (the conclusion is based on the shapes of the light curves) and 2 are long-period eclipses. The remaining 37 are of yet uncertain

type due to our short observational run; because of the limited span of observations, the reliable determination of periods was limited to periods of  $\leq 0.1$  days. Our results constitute the largest population of variables discovered in one research work on M53. Compared to the latest photometric study of this cluster by Dekany & Kovacs (2009), our photometry depth reaches 21 magnitude in *R*, has better precision and better resolution. Consequently, we were able to identify many more new variables and, in a few cases, clarify the status of previously reported ones. We have shown that some previously known variables are misidentified, and some are even non-variable. We also have shown that stars previously thought to be photometrically stable (Stetson 2000) can display short-period variability and that status of some of them as photometric standards possibly have to be revised. We refined the equatorial coordinates for all previously known variables in our FOV and provided the equatorial coordinates and finding charts for newly discovered variable candidates. We also report the error in the listing of the M53 variables coordinates in the online catalogue

TABLE 9  
EQUATORIAL COORDINATES ( $\alpha, \delta$ ) AND LIGHT CURVE PARAMETERS FOR NEW UNCLASSIFIED VARIABLE STARS IN M53.

Variable designation	$\alpha(2000)$ (h:m:s)	$\delta(2000)$ ( $^{\circ}$ : ' : ")	Period (d)	$\langle R \rangle$ (mag)	Remarks
VC1	13:12:43.85	18:10:13.0	0.100201	17.099	RR1?
VC2	13:12:50.58	18:10:18.9	0.207101	18.511	
VC3	13:12:50.66	18:09:39.3	0.121557	19.713	
VC4	13:12:50.96	18:10:27.3	0.298433	20.637	
VC5	13:12:52.26	18:10:21.3	0.118212	18.967	BSS acs#201010
VC6	13:12:52.45	18:09:37.3	0.089110	18.861	
VC7	13:12:52.50	18:10:13.6	0.147758	19.105	
VC8	13:12:52.83	18:10:00.8	0.097510	18.835	
VC9	13:12:53.36	18:09:31.6	0.110812	18.430	RR1?
VC10	13:12:53.61	18:09:54.4	0.210301	17.597	
VC11	13:12:54.44	18:10:31.2	0.096401	18.703	
VC12	13:12:54.76	18:10:10.4	0.124401	17.855	
VC13	13:12:55.32	18:10:21.7	0.177668	17.237	BSS pc#100221
VC14	13:12:55.42	18:10:39.0	0.190400	19.127	
VC15	13:12:55.71	18:09:57.0	0.188068	18.470	
VC16	13:12:55.84	18:10:35.5	0.233201	17.284	
VC17	13:12:56.05	18:09:59.5	0.185700	18.463	BSS pc#103149
VC18	13:12:56.38	18:10:52.1	0.095901	20.072	
VC19	13:12:56.43	18:10:57.7	0.149258	20.155	
VC20	13:12:56.59	18:10:47.5	0.089911	17.869	
VC21	13:12:56.93	18:10:30.1	0.180000	18.741	LPV
VC22	13:12:56.95	18:11:02.1	0.202601	19.666	
VC23	13:12:57.09	18:10:15.8	0.065368	18.776	
VC24	13:12:57.66	18:10:50.0	0.298433	19.978	
VC25	13:12:58.02	18:09:06.8	0.157258	19.777	W UMa?
VC26	13:12:58.03	18:09:03.1	0.115912	19.530	
VC27	13:12:58.07	18:09:23.5	0.083209	18.702	
VC28	13:12:53.09	18:10:08.7	0.065629	19.080	
V57_3	13:12:57.56	18:10:12.8	0.1800	16.7022	BSS acs#1200729 BSS pc#102387
V80_7	13:12:55.53	18:09:56.9	0.104911	19.575	

NOTE.—The periods are derived from incomplete light curves and are only approximate due to the short span of our observations.

TABLE 10

BLUE STRAGGLERS IN M53. COLUMN (1) IS THE STAR NUMBER FROM BSS CATALOGUE BECCARI ET AL. (2008). FOR PREVIOUSLY KNOWN SX PHE WE RETAINED THE USUAL NOMENCLATURE (CLEMENT ET AL. 2001). NEW BSS ARE ARE DESIGNATED AS FOLLOWS: SX MEANS SX PHE-TYPE STARS, W MEANS W UMA-TYPE STARS, E STANDS FOR ECLIPSE AND VC STANDS FOR VARIABLE CANDIDATE (TYPE YET UNIDENTIFIED).

Cat#BSS	Variable	$V_{\text{Bec}}$ (mag)	$\langle R \rangle$ (mag)	$P_{\text{LK}}$ (d)	Type	Remarks
lbc#208210	V74	19.2848	19.054	0.045055	SXPhe	first report by DK
lbc#219783	V75	19.5750	19.455	0.044178	SXPhe	new match
lbc#213681	V76	19.8584	19.434	0.041467	SXPhe	first report by DK
lbc#231344	V79	19.7637	19.183	0.046255	SXPhe	first report by DK
lbc#208804	V89	19.6853	19.435	0.043278	SXPhe	new match
acs#102387	V87	18.8752	19.356	0.046855	SXPhe	new match
pc#102387	V57_3	18.8752	16.7022	0.1784	?	see Sec. 3.1.1
acs#200309	SX4	19.2108	19.4494	0.049500	SXPhe	new
acs#200279	SX6	19.1799	18.1171	0.044755	SXPhe	new
acs#200174	SX9_1	19.0312	18.5738	0.054056	SXPhe	new
acs#1200685	SX14	18.3878	18.6844	0.071130	SXPhe	new
acs#100512	SX17	19.3060	18.0077	0.040567	SXPhe	new
acs#100732	SX19	19.5009	19.3035	0.044378	SXPhe	new
acs#100681	SX21	19.4517	19.5682	0.037762	SXPhe	new
lbc#238275	SX2	19.8489	19.6018	0.039362	SXPhe	new
lbc#240911	SX3	18.9840	18.7855	0.059824	SXPhe	new
acs#100496	W9	19.2661	19.369	0.152667	WUMa?	new
acs#101000	E3	19.6599	19.439	0.24482	EW/EB?	new
acs#201010	VC3	19.7295	19.713	0.121557	?	new
acs#1200729	VC28	18.5123	19.080	0.065629	?	new
pc#100221	VC13	19.5517	17.237	0.177668	?	new
pc#103181	VC15	19.1203	18.470	0.188068	?	new
pc#103149	VC17	19.0852	18.463	0.185700	?	new

NOTE.— $P_{\text{LK}}$  means the period was obtained by LK method (see Sec. 4.4) and in some cases is only approximate due to the short span of our observations.

by Samus.

Our study shows that M53 has a number of variable stars comparable to M15, the most populous cluster in variables; however, we feel that we have barely scratched the surface. Extensive tests would be necessary to answer the question about the number of variables which were missed. We are confident that with the advent of new differential imaging technique, using 2-m class telescopes and regular observations with moderate cadence, it will be possible to discover many more variables in this cluster.

## REFERENCES

- Alard, C. 2000, *A&AS*, 144, 363
- Alard, C. & Lupton, R. H. 1998, *ApJ*, 503, 325
- Arellano Ferro, A., Giridhar, S., Rojas López, V., Figuera, R., Bramich, D. M., & Rosenzweig, P. 2008, *Rev. Mexicana Astron. Astrofis.*, 44, 365
- Beccari, G., Lanzoni, B., Ferraro, F. R., Pulone, L., Bellazzini, M., Fusi Pecci, F., Rood, R. T., Giallongo, E., Ragazzoni, R., Grazian, A., Baruffolo, A., Bouche, N., Buschkamp, P., De Santis, C., Diolaiti, E., Di Paola, A., Farinato, J., Fontana, A., Gallozzi, S., Gasparo, F., Gentile, G., Pasian, F., Pedichini, F., Smareglia, R., Speziali, R., Testa, V., & Vernet, E. 2008, *ApJ*, 679, 712
- Bramich, D. M. 2008, *MNRAS*, 386, L77
- Bramich, D. M., Figuera Jaimes, R., Giridhar, S., & Arellano Ferro, A. 2011, *MNRAS*, 413, 1275
- Bramich, D. M., Horne, K., Bond, I. A., Street, R. A., Cameron, A. C., Hood, B., Cooke, J., James, D., Lister, T. A., Mitchell, D., Pearson, K., Penny, A., Quirrenbach, A., Safizadeh, N., & Tsapras, Y. 2005, *MNRAS*, 359, 1096
- Clement, C. M., Muzzin, A., Dufton, Q., Ponnampalam, T., Wang, J., Burford, J., Richardson, A., Rosebery, T., Rowe, J., & Hogg, H. S. 2001, *AJ*, 122, 2587
- Cook, K. H. 2006, *Journal of the American Association of Variable Star Observers (JAAVSO)*, 35, 29
- Dekany, I. & Kovacs, G. 2009, *VizieR Online Data Catalog*, 350, 70803
- Evstigneeva, N. M., Samus', N. N., & Alcaïno, G. 1997, *Astronomy Letters*, 23, 395
- Hartman, J. D., Bakos, G., Stanek, K. Z., & Noyes, R. W. 2004, *AJ*, 128, 1761
- Hartman, J. D., Gaudi, B. S., Holman, M. J., McLeod, B. A., Stanek, K. Z., Barranco, J. A., Pinsonneault, M. H., & Kalirai, J. S. 2008, *ApJ*, 675, 1254
- Jeon, Y., Lee, M. G., Kim, S., & Lee, H. 2003, *AJ*, 125, 3165
- Jeon, Y.-B., Lee, M. G., Kim, S.-L., & Lee, H. 2004, *AJ*, 128, 287
- Kopacki, G. 2000, *A&A*, 358, 547
- Lafler, J. & Kinman, T. D. 1965, *ApJS*, 11, 216
- Lomb, N. R. 1976, *Ap&SS*, 39, 447
- McNamara, D. H. 2000, *PASP*, 112, 1096
- Nandra, K., George, I. M., Mushotzky, R. F., Turner, T. J., & Yaqoob, T. 1997, *ApJ*, 476, 70
- Press, W. H., Teukolsky, S. A., Vetterling, W. T., & Flannery, B. P. 1992, *Numerical recipes in FORTRAN. The art of scientific computing* (Cambridge: University Press, —c1992, 2nd ed.)
- Rodríguez, E. & López-González, M. J. 2000, *A&A*, 359, 597
- Safonova, M. & Shastri, P. 2010, *Ap&SS*, 325, 47
- Safonova, M. & Stalin, C. S. 2010, *New Astronomy*, 15, 450
- Schlegel, D. J., Finkbeiner, D. P., & Davis, M. 1998, *ApJ*, 500, 525
- Stetson, P. B. 2000, *PASP*, 112, 925
- Tamuz, O., Mazeh, T., & North, P. 2006, *MNRAS*, 367, 1521
- Tamuz, O., Mazeh, T., & Zucker, S. 2005, *MNRAS*, 356, 1466
- Vaughan, S., Edelson, R., Warwick, R. S., & Uttley, P. 2003, *MNRAS*, 345, 1271

Zinn, R. 1985, ApJ, 293, 424